aerospace

MDPI

Article

Lightweight Design for Active Small SAR S-STEP Satellite Using Multilayered High-Damping Carbon Fiber-Reinforced Plastic Patch

Kyung-Rae Koo [1,2], Hyun-Guk Kim [1], Dong-Geon Kim [1], Seong-Cheol Kwon [1] and Hyun-Ung Oh [3,4,*]

[1] Yongin R&D Center, Hanwha Systems, 491-23, Gyeonggidong-ro, Namsa-myeon, Cheoin-gu, Yongin-si 17121, Republic of Korea; kr.koo@hanwha.com (K.-R.K.); hyunguk1.kim@hanwha.com (H.-G.K.); dgkim90@hanwha.com (D.-G.K.); seongcheol.kwon@hanwha.com (S.-C.K.)
[2] Department of Integrated Space Defense, Yonsei University, 50 Yonsei-ro, Seodaemun-gu, Seoul 03722, Republic of Korea
[3] STEP Lab. Ltd., 236-3 Bongyong-dong, Yuseong-gu, Daejeon City 34202, Republic of Korea
[4] School of Aerospace & Mechanical Engineering, Korea Aerospace University, 76 Hangggongdaehak-ro, Deogyang-gu, Goyang-si 10540, Republic of Korea
* Correspondence: ohu129@kau.ac.kr

Abstract: In the launch environment, satellites are subjected to severe dynamic loads. These dynamic loads in the launch environment can lead to the malfunction of the payload, or to mission failure. In order to improve the structural stability of satellites and enable the reliable execution of space missions, it is necessary to have a reinforcement structure that reduces structural vibrations. However, for active small SAR satellites, the mass requirements are very strict, and this makes it difficult to apply an additional structure for vibration reduction. Therefore, we have developed a carbon fiber-reinforced plastic (CFRP)-based laminated patch to obtain a vibration reduction structure with a lightweight design for improving the structural stability of an S-STEP satellite. To verify the vibration reduction performance of the CFRP-based patch, sine and random vibration tests were conducted at the specimen level. Finally, the structural stability of the S-STEP satellite with the proposed CFRP-based laminated patch was experimentally verified using sine and random vibration tests. The validation results indicate that the CFRP-based laminated patch is an efficient solution which can effectively reduce the vibration response without the need for major changes to the design of the satellite structure. The lightweight vibration reduction mechanism developed in this study is one of the best solutions for protecting vibration-sensitive components.

Keywords: synthetic aperture radar (SAR); Small SAR Technology Experimental Project (S-STEP); carbon fiber-reinforced polymer (CFRP); CFRP-based patch

Citation: Koo, K.-R.; Kim, H.-G.; Kim, D.-G.; Kwon, S.-C.; Oh, H.-U. Lightweight Design for Active Small SAR S-STEP Satellite Using Multilayered High-Damping Carbon Fiber-Reinforced Plastic Patch. *Aerospace* **2023**, *10*, 774. https://doi.org/10.3390/aerospace10090774

Academic Editor: Angelo Cervone

Received: 29 June 2023
Revised: 18 August 2023
Accepted: 30 August 2023
Published: 31 August 2023

1. Introduction

The new space paradigm has affected the development philosophy of space engineering worldwide. This paradigm involves a global and progressive commercialization of the space sector led by private companies rather than government-funded agencies [1,2]. This acceleration is being driven by the influence of faster, cheaper, and lighter space technology. In particular, the emergence of small satellite constellations is playing a significant role in the new space paradigm. Compared with traditional large-scale satellites, the design, evaluation, and launch processes of clusters of small artificial satellites are much faster, enabling the simultaneous launching of multiple satellites and dramatically reducing launch costs. Furthermore, recent advancements in manufacturing technology have made the mass production of satellites possible. Due to these advantages, the small SAR satellite platform is extensively utilized for challenging missions such as real-time remote sensing, fast telecommunications, and global internet connectivity [3–5].

All artificial satellites are subjected to various dynamic loads during the launch process [6,7]. These mechanical loads are caused by factors such as static acceleration from engine thrust, sine vibrations from engine cutoff, and self-induced vibrations from the incomplete combustion of propellant. Additionally, thrust noise induces random vibrations, and the separation process between the launch adaptor and the satellite generates mechanical shock. Moreover, combustion noise from the burning of fuel and aerodynamic noise caused by friction with the air during the launch process create broadband acoustic noise within the satellite fairing [8–11]. This high-frequency noise is a primary source of severe vibrations in the satellite. Due to the complexity and severity of these dynamic loads, they can become critical factors leading to launch failures and component malfunctions. Therefore, ensuring structural stability against vibrations in the launch environment through appropriate mechanical design is essential to increase the success rate of space missions for satellites.

To ensure structural stability against the external loads caused by the launch environment, Kwon et al. applied a laminated vibration damping structure based on FR-4 and a viscoelastic layer to the satellite and payload [12]. In 2017, a blade-type vibration isolator with a laminated vibration reduction structure was developed to reduce vibrations from a cooler, and this exhibited higher vibration attenuation performance than the existing titanium structure [13]. Additionally, Park et al. designed a highly damped PCB board using a laminated structure with viscoelastic tape. This PCD board improved the fatigue life of the vibration-sensitive electronic units within the satellite [14]. Furthermore, in 2022, Kim et al. experimentally validated the vibration attenuation performance of a laminated vibration isolator based on a laminated structure for SAR satellites by exposing it to random vibrations and acoustic loads [5].

Due to the launch environment, weight/volume increases arising from structural design changes cannot safely be accommodated, so the mass requirement for the development of a small satellite is very specific. In this context, an attachable vibration reduction patch is an affordable solution that can be implemented without major design changes. However, no study has yet been conducted in which this type of patch has been attached to the main structure of a small satellite weighing around 100 kg to demonstrate the overall vibration reduction performance of the satellite. Therefore, we proposed a multilayered high-damping CFRP-based patch made using a carbon fiber-reinforced polymer for attenuating the launch vibration loads transmitted to an X-band active small SAR satellite called the S-STEP (Small SAR Technology Experimental Project) and improving the structural stability of its primary structure.

Typically, fiber-reinforced composites consist of fibers arranged in a specific direction and immersed in a resin [15]. In the proposed concept, resin bonds the fibers so that their arrangement is kept constant, acts as a damper to reduce the structural vibration response, and allows the load to be transmitted to each fiber when a load is applied [16,17]. Moreover, fiber-reinforced composites can provide outstanding material properties at a light weight. For these structural characteristics, fiber-reinforced composites can provide outstanding material properties at a light weight. Among fiber-reinforced composites, carbon fiber-reinforced polymer (CFRP) is commonly used for space structures that require high stiffness, while aramid fiber- or glass fiber-reinforced composites are utilized for applications that require electrical insulation or radio wave penetration, such as the solar panels and antenna in a satellite system. Additionally, a sandwich-structured composite material consisting of CFRP and honeycomb panels has been widely used because it can withstand the vibrational loads to which the main structure is subjected during the launch process [18,19].

The multilayered, high-damping CFRP-based patch consists of damping tape inside a CFRP plate. Compared with the PCB-based laminated patch that has been used in existing research, the high-damping CFRP-based patch has good mechanical properties because it has relatively high stiffness and can withstand the loads and vibrations generated in the launch environment. Moreover, the high-damping CFRP-based patch is characterized

by the fact that vibrations are damped by the viscoelasticity of the resin in the first place and by the damping tape inside the patch in the second place. In other words, vibrations transmitted to the patch are stored in the form of strain energy and then converted into heat energy by the viscoelastic behavior of the resin and the damping tape.

In this study, an experimental investigation of the vibration reduction performance of a CFRP-based patch was conducted to verify the structural stability of the main structures and on-board units and instruments of a satellite. By utilizing the proposed laminated patch, the structural stability of the satellite could be ensured by attenuating launch vibration excitations. This is expected to have a significant impact on the successful execution of future space missions.

The remainder of this paper is structured as follows: Section 2 provides a general description of the X-band active small SAR satellite S-STEP. Section 3 presents the results of specimen tests evaluating the vibration attenuation performance of the composite material patch and the laminated vibration damping patch based on FR-4. Section 4 showcases the results of random vibration tests conducted on a satellite with the composite material patch attached.

2. An Overview: Active Small SAR S-STEP Satellite

2.1. Introduction to the STM of the S-STEP Satellite

The Small SAR Technology Experimental Project (S-STEP) refers to a project aimed at designing, evaluating, and manufacturing a small SAR satellite based on the new space paradigm. Its objective is to establish a smaller, lighter, faster, and more compact process for obtaining high-resolution images for purposes such as environmental investigations, surface mapping, and disaster monitoring [3–5].

Figure 1 illustrates the operational concept and mission of the S-STEP satellite. The S-STEP satellite encompasses several operational modes, including ScanSAR, VideoSAR, and stripmap modes, each of which offers different resolutions and capabilities, depending on mission requirements [3,4]. The ScanSAR and VideoSAR modes provide resolutions of 1 m and 4 m, respectively, enabling the tracking of various conditions or interesting targets. The high-resolution stripmap mode offers a 1 m resolution and enables wide-area surveillance. Images and videos obtained through the SAR antenna are stored in the bus platform and transmitted to the ground at a speed of 1 Gbps through the X-band antenna. Furthermore, the inter-satellite link (ISL) in the S-band improves the communication capabilities of the satellite constellation and enhances mission capabilities at the system level. The key performance parameters of the S-STEP satellite are presented in Table 1. As is depicted in Figure 1b,c, the S-STEP satellite is a compact plate-type satellite weighing around 80 kg [3]. The S-STEP satellite exhibits exceptional performance relative to its mass.

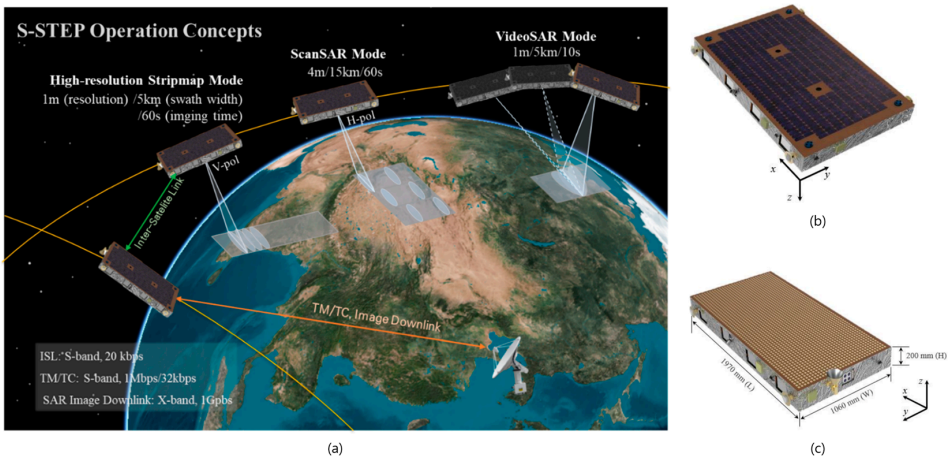

Figure 1. Schematic of active small SAR S-STEP satellite: (**a**) S-STEP operational concept and mission; (**b**) view from −Z side (solar array); (**c**) view from +Z side (SAR antenna) [4].

Table 1. System specifications of the active small SAR S-STEP satellite [4].

Specification		Value
Mission lifetime		3 years
Mass		80.3 kg
Satellite size		2000 × 1100 × 200 mm (under)
Power	Generation	340 W
	Stored (battery)	648 Wh
Inter-satellite link		RF (X-band)
TMTC/image downlink		S-band/X-band
Pointing accuracy		0.085°
Resolution (25°)		1 m (Stripmap) 4 m (ScanSAR) 1 m (VideoSAR)
Swath (elevation × azimuth)		5 × 420 km (Stripmap) 15 × 420 km (ScanSAR) 5 × 5 km (VideoSAR)
Image acquisition time		60 s (Stripmap) 10 s (VideoSAR)

2.2. Launch Environment of the S-STEP Satellite

During the launch process in which a satellite is placed into an on-orbit environment, the launch vehicle is subjected to external loads due to factors such as airflow, rocket–stage separation, and fuel combustion. The mechanical loads imposed on the satellite housed within the launch vehicle fairing in the launch environment consist of harmonic vibration loads, random vibration loads, and acoustic loads. In order to consider these various dynamic loads, the launch environment is separated into individual loads for analysis and evaluation [20]. Acoustic loads result from interactions between the fairing and the atmosphere, where aerodynamic noise is transmitted into the interior of the launch vehicle, creating a resonant sound field. Random and sine vibration loads propagate into the satellite through the interface with the launch adaptor. Sine vibration loads, typically within the frequency range of 5–100 Hz, are critical considerations during the preliminary design steps as they manifest as excessive vibrations. Random vibration loads occur due to various dynamic loads, such as the operation of the rocket engine, aerodynamic excitation, etc. Additionally, during rocket–stage separation, the launch vehicle is subjected to a large load for a very short duration, and this is transmitted to the satellite as an impulse load. As the launch vehicle accelerates, the artificial satellite is subjected to quasi-static loads due to gravitational forces. Because the S-STEP satellite has an elongated structure in the direction lateral to the launch direction, the bending mode is dominant regardless of the launch direction. Additionally, despite its small size, the satellite has a large surface area, making it vulnerable to the acoustic environment. The disadvantage of adding reinforcements to solve this problem is a significant increase in mass.

To ensure structural resilience against these dynamic loads occurring in the launch environment, a laminate composite structure-based patch was fabricated and applied to the satellite. Using an anti-resonance design, it is possible to dramatically mitigate the response to specific vibration modes caused by sine vibration loads that occur below 100 Hz. However, it is challenging to apply an anti-resonance design that will mitigate the effects of random vibrations and acoustic loads, which occur in broader frequency ranges of 0–2 kHz and 0–8 kHz, respectively. Due to the broad frequency ranges of random and acoustic loads, it is hard to determine the specific vibrating mode that is contributing to the entire frequency band. Designing vibration reduction structures using composite materials is an effective approach to attenuating vibration responses in the broadband frequency

range because the high damping and stiffness properties of the viscoelastic and composite materials can mitigate random loads. By utilizing the CFRP-based patch proposed in this study, it will be possible to develop a lightweight structure with high stiffness that will improve structural stability at the satellite system level and ensure a high level of structural reliability against dynamic loads.

3. Vibration Reduction Performance of Multilayered Laminated Composite Structure

3.1. Brief Description of CFRP Laminated Patch for Vibration Reduction

The laminated patch proposed in this study is composed of a carbon fiber-reinforced polymer with a viscoelastic structure. The viscoelastic structure is composed of a damping layer and a constrained layer. The damping layer, made from damping tape, dampens structural vibrations by converting a portion of the strain energy into heat. However, a laminated patch attached to the host structure can cause shear vibrations in the in-plane shear direction due to the difference in shear stiffness between the host structure and the laminated patch. Therefore, the shear strength of both the host structure and the laminated patch should be measured experimentally.

Figure 2 illustrates the dimensional configuration and fabrication process of the laminated patch. The laminated patch is produced by cross-laminating damping tape (specifically, 3M 966 adhesive tape) and CFRP or FR4 plates. As is shown in Figure 2a, the fabricated laminated patch is attached to the front and rear sides of the host structure. Figure 2b shows the fabrication process of the laminated patch. First, alcohol disinfectant wipes are used to remove impurities from each layer of carbon fiber-reinforced polymer (CFRP). Adhesive tape is then cut to the same size as the attachment layer. Following the stacking sequence, each layer is laminated using the hand layup method, and the entire structure is pressurized using a steel plate with eight bolts that are tightened to a specific torque for 12 h to complete the lamination structure.

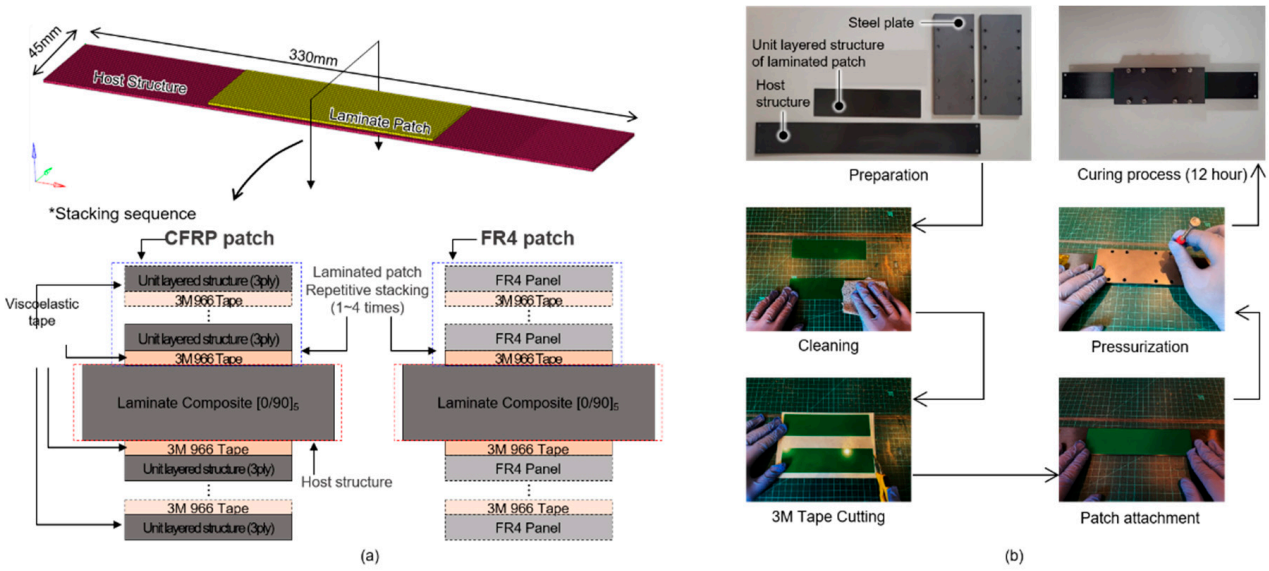

Figure 2. Fabrication process of CFRP-based patch: (**a**) dimensions and configuration of the specimen; (**b**) hand layup process for CFRP-based patch.

3.2. Sine and Random Vibration Tests Conducted on CFRP- and FR4-Based Patches

Figure 3 shows the experimental setups of the sine and random vibration tests. The host structures, which are the target of the structural vibration reduction, are composed of carbon fiber-reinforced polymer (CFRP) of FR4 panels. The material used for the host structure is same as that of the skin of the aluminum honeycomb panel applied to the satellite structure. The specimen size was selected according to the frequency range in which the vibration of the satellite body would increase most significantly. The S-STEP

satellite (the subject of this study) exhibited the highest modal mass and vibration response at a vibration frequency of 80 Hz. At this frequency, the z-directional PSD response at the center of gravity (CoG) of the STM of the S-STEP satellite reached its maximum value [3]. This mode is located within the frequency ranges of both the sine and random vibration excitations mentioned above. Therefore, the host structure used in the specimen test was a laminated structure fabricated using a CP125N UD prepreg with dimensions of 330 mm × 45 mm and a fundamental mode at 90 Hz. As is shown in Figure 3a, the host structure without a laminated patch exhibited a fundamental mode near 80 Hz. As is shown in Figure 3b, four interface points were considered for the CFRP-based patch specimen test. The sine and random vibration tests for the FR4-based patch specimen were implemented using same test configuration. The specifications of the sine and random vibration loads used in the CFRP-based patch specimen test were derived from the results of the random and sine vibration analyses of the S-STEP satellite. Performing a sine vibration analysis of the S-STEP satellite along the z-axis resulted in a maximum shear stress of 5.2 MPa in the satellite structure. To generate a maximum shear stress of 5.2 MPa at the specimen level, a maximum sinusoidal vibration load of 6.75 g was required. Additionally, for the random vibration loading, a maximum random vibration profile input of 0.31 g^2/Hz was needed.

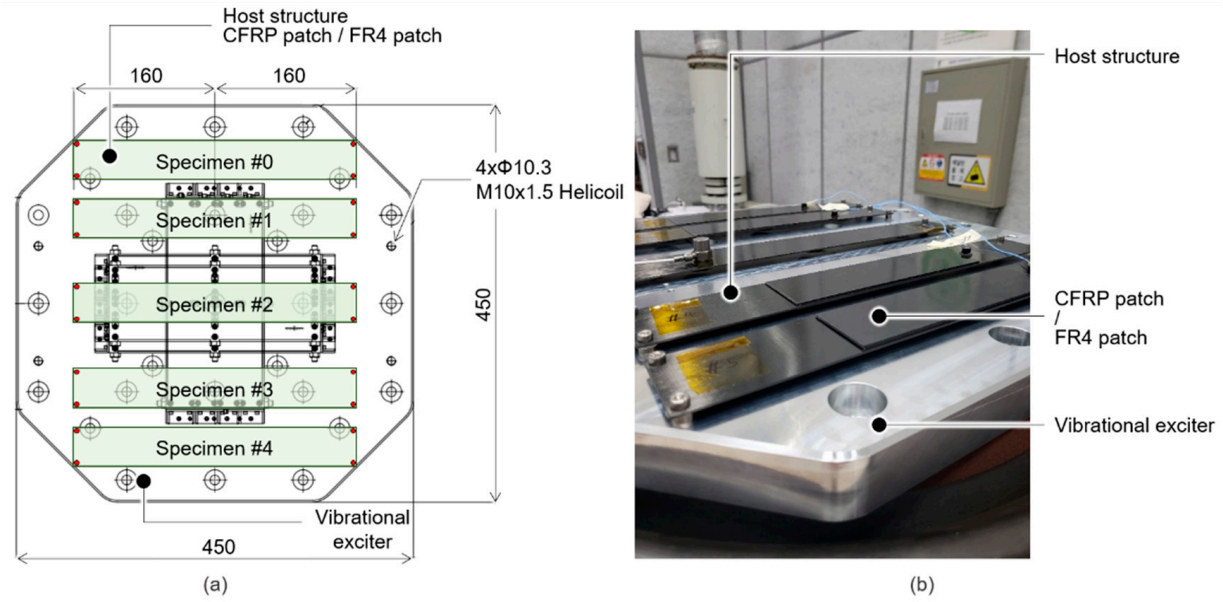

Figure 3. Configuration of sine and random vibration tests: (**a**) test configuration; (**b**) experimental setup.

Table 2 presents the weights of the specimens with the CFRP- and FR4-based patches according to each stacking sequence used in the specimen tests. As was mentioned in Section 3.1, the host structure was a CFRP panel with a (0/90)5 laminated pattern. The CFRP-based patch consisted of a unit layer with a (0/90/0) laminated pattern which was laminated onto the upper and lower surfaces of the host structure in one to four layers, resulting in five test specimens with different stacking sequences. In the case of the FR4-based patch, a 0.4 mm thick FR4 panel was applied to the laminated pattern. The FR4-based patch consisted of a unit layer with an FR4 panel which was laminated onto the upper and lower surfaces of the host structure in one to four layers.

Figure 4 illustrates the vibration responses of each specimen to the sinusoidal and random vibration loads defined in Figure 4d. The specifications of the sine and random vibrations are shown in Tables 3 and 4, respectively. As Figure 4a shows, the influence of the dominant vibration modes at 31, 47, and 93 Hz diminished in the specimens with the CFRP-based patch for each stacking sequence. Reductions in the peak responses at the resonance frequency were observed even when the FR4-based patch was applied. Additionally, the acceleration response of the host structure without any type of patch

exhibited a high value of 88 g due to the vibration mode at 95 Hz. However, the acceleration responses of specimens #1 to #4 with the FR4-based patches decreased to 14.8, 15.9, 25.9, and 14.2 g, respectively. The acceleration responses of specimens #1 to #4 with the CFRP-based patches also decreased (to 40.9, 29.7, 28.8, and 17.2 g, respectively). As Figure 4a shows, the results for the CFRP-based patch show that the sine vibration reduction performance of the laminated patch reached as much as 80% (#4). According to the results of the sine vibration tests for the FR4-based patch (shown in Figure 4b), despite the overall increase in mass due to the stacking of the plates, there was no significant correlation between the vibration reduction in the host structures with FR4-based patches and the stacking sequence. As is shown in Figure 4c,d, the random vibration responses were significantly reduced in the specimens with the laminated patches compared with the host structure. As Figure 4c shows, the random vibration response of the host structure without the laminated patch showed a value of 46.1 grms in the 20 to 2000 Hz frequency range, while the random vibration responses of specimens #1 to #4 with the CFRP-based patches decreased to 27.0, 20.5, 14.8, and 9.5 grms, respectively. These results indicate that the random vibration reduction performance of the CFRP-based patch was 79% overall (#4), and the vibration reduction performance of the CFRP-based patch was therefore higher than that of the FR4-based patch (Figure 4d).

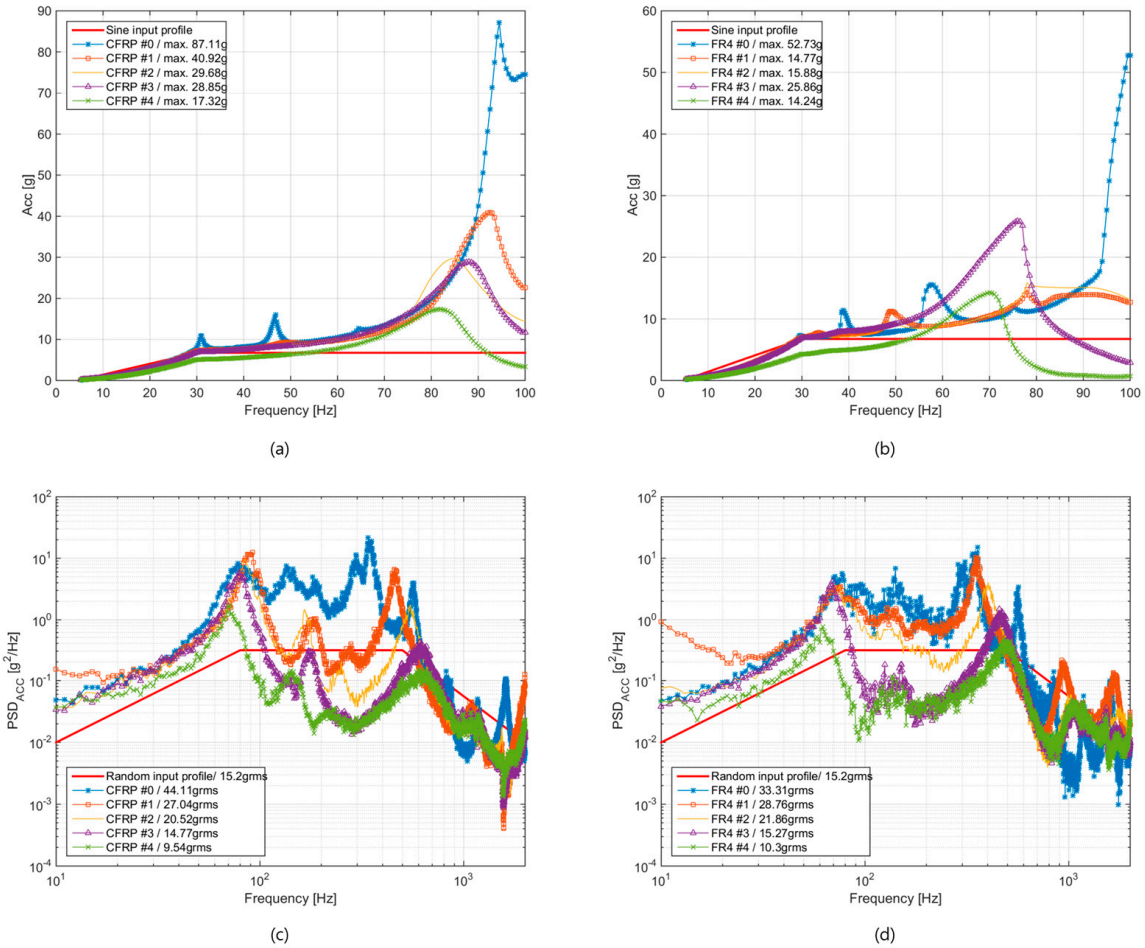

Figure 4. Sine and random vibration tests for specimens with and without CFRP- and FR4-based patches (#0–#4): results of sine vibration tests with and without (**a**) CFRP-based and (**b**) FR4-based patches along the z-direction; results of random vibration tests with and without (**c**) CFRP-based and (**d**) FR4-based patches along the z-direction.

Table 2. Masses and stacking sequences of CFRP- and FR4-based laminated patch specimens and host structures.

Material Type	Host Structure (45 mm × 330 mm)		Laminated Patch (42 mm × 160 mm)	
	No.	Stacking Sequence	Stacking Sequence	Mass (g)
CFRP	#0	$(0/90)_5$	-	28.2
	#1		(0/90/0)1	36.5
	#2		(0/90/0)2	44.7
	#3		(0/90/0)3	52.8
	#4		(0/90/0)4	61.3
FR4	#0	$(0/90)_5$	-	28.2
	#1		0.4 mm*1	40.1
	#2		0.4 mm*2	52.1
	#3		0.4 mm*3	63.7
	#4		0.4 mm*4	75.5

Table 3. Specifications of sine vibration inputs for specimen tests along the z-direction.

Frequency	Sine Vibration Input (g)
0	0
30	6.75
100	6.75

Table 4. Specifications of random vibration inputs for specimen tests along the z-direction.

Frequency	Random Vibration Input (g^2/Hz)
20	0.01
80	0.31
500	0.31
2000	0.01

The laminated patches in the composite material disperse the flow of vibrational energy entering the structure, leading to a significant reduction in the structural response to dynamic loads. The results of the tests outlined in this section demonstrate that the CFRP-based patch dramatically reduces the vibration response of the structure for both sine and random vibration loads and improves the structural stability of the host structure. Because of its effect on the structural mass and its vibration reduction performance, the stacking sequence of specimen #3 with the CFRP-based patch was used in the S-STEP satellite to reduce both the sine and random vibrations.

Figure 5 shows the performance evaluations of the FR-4- and CFRP-based laminate patches described in Table 2. The left and right axes show the frequency/mass and damping ratios calculated during the specimen tests with respect to the FR4- and CFRP-based laminated patches. As Figure 5 shows, the maximum vibration reduction performance value was obtained using patch #4, which was the thickest and heaviest structure (see Table 2). Although the damping ratio was increased with respect to the thickness of the laminated patch, patch #4 had the lowest frequency/mass ratio. We therefore adopted specimen #3 with the CFRP-based patch.

3.3. Lap Shear Testing of CFPR-Based Laminated Patch

Lap shear tests were conducted to assess the shear strength of the CFRP-based patch. Figure 6 illustrates the experimental setup used for the lap shear tests. As Figure 6a shows, the lap shear tests were performed using standard specimens in accordance with ASTM D5868 [21]. The specimens were fixed using a clamping jaw while a load was applied to the opposite end to measure the load at which delamination occurred in the adhesive region.

The individual specimens were comprised of a CFRP plate and a CP125N unidirectional prepreg with a $(0/90/0)_4$ stacking sequence. Each specimen was 25 mm wide and 100 mm long. Each specimen was attached to a 25 mm × 25 mm area using viscoelastic tape (3M 966 tape). The lap shear test was repeated three times for each specimen, resulting in delamination at an average shear strength of 8.28 MPa. Considering the fact that the maximum shear stress observed during the sine vibration analysis was 5.2 MPa, the laminated patch demonstrated structural stability in terms of secondary bonding in launch environments. In light of the experimental results obtained from the vibration and lap shear tests, we decided to apply the CFRP-based patch to the S-STEP satellite and evaluate its vibration reduction performance.

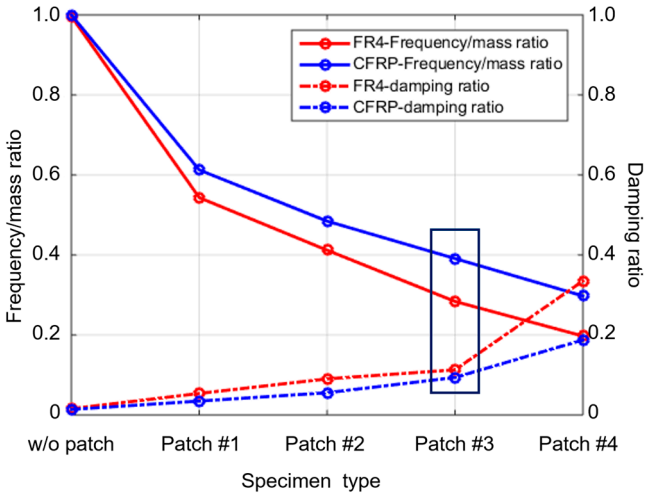

Figure 5. Performance evaluations of the FR-4 and CFRP-based laminate patches described in Table 2.

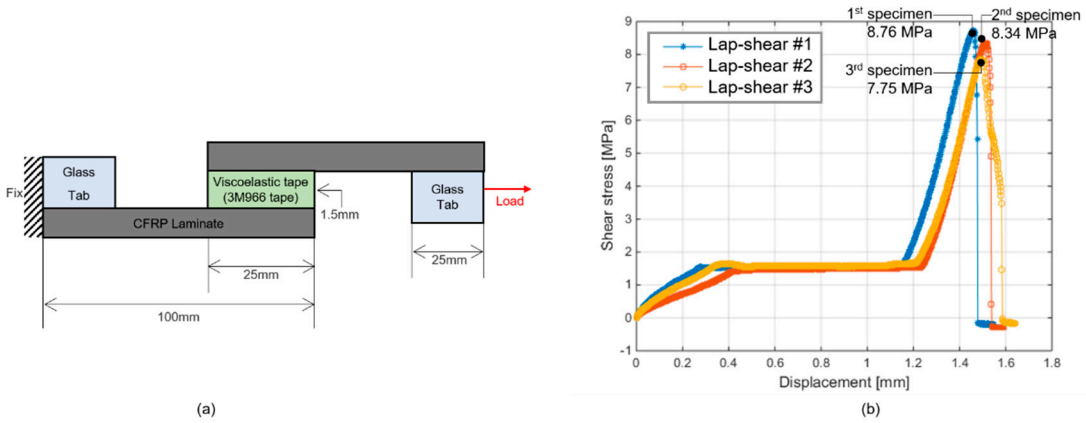

Figure 6. Lap shear testing of CFRP-based patch: (**a**) test configuration based on ASTM D5868; (**b**) shear stress required for delamination between two CFRP plates.

4. Numerical and Experimental Verification of Vibration Reduction Performance of CFRP-Based Patch for S-STEP Satellite

4.1. Structural Analysis of S-STEP Satellite with CFRP-Based Patch

In this section, the random vibration test that was conducted on the S-STEP satellite is described. In order to evaluate the response of the satellite, this section discusses the vibration analysis of the S-STEP satellite, incorporating the material properties of the laminated patch derived from the specimen tests outlined in Section 3. As is shown in Figure 7, the vibration reduction performance of the laminated patch increased as the number of lamination layer increased. However, it should be noted that the structural mass also increased. After considering the trade-off between the vibration reduction performance

and the structural mass, it was decided that the stacking sequence of specimen #3 would be applied to the satellite structure. Figure 7 illustrates the configuration and the results of the sine vibration analysis of the S-STEP satellite with and without the CFRP-based patch. Due to its plate-like structural characteristics, the S-STEP satellite exhibited the largest vibration response along the z-direction. Therefore, a sine vibration analysis was performed specifically for the z-axis vibration response. Figure 7 shows the sine vibration analysis setup and the stress distribution at the peak frequency. As is shown in Figure 7a, the S-STEP satellite is subjected to a maximum sine vibrational load of 1.25 g through the interface with the launch adaptor located on the solar panel side. Figure 7b shows the acceleration results of the sine vibration analysis of the S-STEP satellite. At the peak frequency, the acceleration response of the satellite without the CFRP-based patch was 26.8 g higher than the design load (18 g). However, the maximum acceleration response of the satellite with the CFRP-based patch was 15.1 g lower than the design load. At the peak frequency, the acceleration response of the satellite with the CFRP-based laminated patch was 43.6% lower than that of the satellite without the laminated patch. Figure 7c shows the stress distribution in the honeycomb panel of the S-STEP satellite connected with launch adaptor at the peak frequency. The maximum stress was generated in the vicinity of the ring-shaped structure in the center of the honeycomb structure. Therefore, a three-layered CFRP-based patch (#3) was applied in each of these four locations.

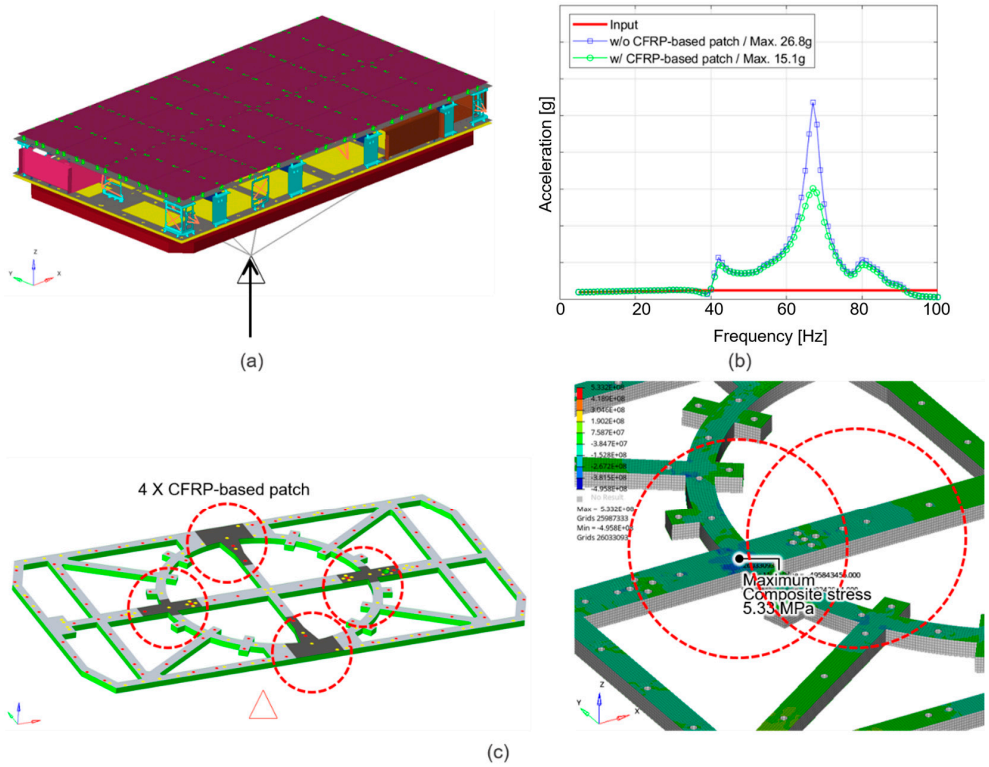

Figure 7. Sine vibration analysis of S-STEP satellite with CFRP-based patch: (**a**) configuration of sine vibration analysis; (**b**) acceleration response at CoG in satellite with and without CFRP-based patch; (**c**) locations of CFRP-based patches and stress distribution in honeycomb structure of satellite with patches.

4.2. Launch Vibration Test of S-STEP Satellite with CFRP-Based Patch

A random vibration test was conducted to experimentally evaluate the vibration reduction performance of the CFRP-based patch. The proposed patches were applied to the surface of the CFRP honeycomb panel in the structural model (SM) of S-STEP satellite. Due to the structural characteristics of the S-STEP satellite, which exhibited the most severe vibration response in the out-of-plane direction, the random vibration test focused on the

z-axis direction. Figure 8 illustrates the setup of the random vibration test in the z-axis direction. The random vibration test was performed on the S-STEP satellite using a random load. Before and after each stage of the random vibration test, a low-level sine sweep (LLSS) test was conducted to detect any structural damage, e.g., frequency shifts or amplitude changes [20].

Figure 8. Setup of sine and random vibration tests performed on the S-STEP satellite along the z-direction using a 300 KN vibrational exciter.

Figure 9 depicts the vibration responses obtained at the satellite's CoG (center of gravity) during 0 dB sine and random vibration tests. As is shown in Figure 9a, the maximum response obtained in the sine vibration test was 15.02 g, which is lower than the design load (18 g). The ability of the structure to mitigate the effects of sine vibrations was thus better with the CFRP-based patch than without it. As is shown in Figure 9b, the input profile of the random vibration test had a value of 6.09 grms, while the vibration responses at the CoG were measured at 5.84 grms, indicating a lower responses compared with the input. According to these test results, the S-STEP satellite with the CFRP-based patch demonstrated high structural stability under random vibration environments (Tables 5 and 6).

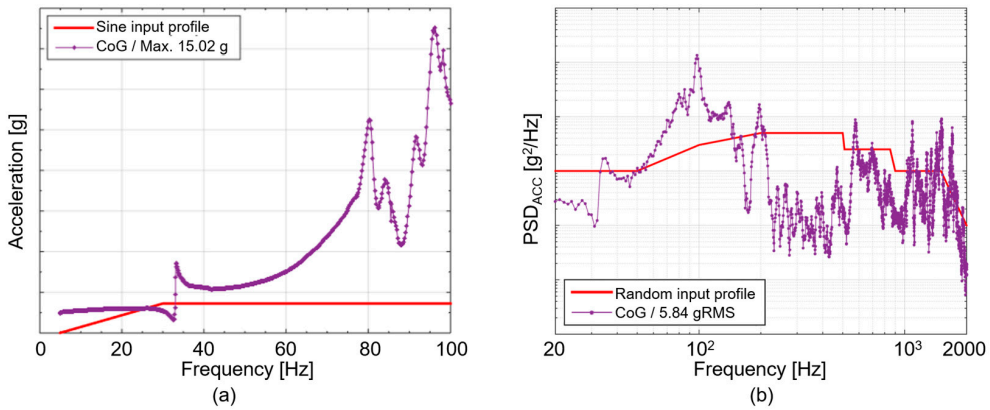

Figure 9. Results of the vibration test at the CoG of the S-STEP satellite with the CFRP-based patch: (**a**) sine vibration tests; (**b**) random vibration tests.

Table 5. Sine vibration input specifications for the satellite test along the z-direction.

Frequency	Sine Vibration Input (g)
5	1.0
35	1.25
100	1.25

Table 6. Random vibration input specifications for the satellite test along the z-direction.

Frequency	Random Vibration Input (g^2/Hz)
20	0.01
50	0.01
100	0.0301
200	0.05
500	0.05
510	0.025
850	0.025
900	0.01
1500	0.01
2000	0.001
Duration: 120 s	
6.09 grms	

Figure 10 presents the results of the LLSS (low-level sine sweep) test that was conducted on the CoG, battery, power supply unit (PSU), and SAR antenna attachment of the satellite before and after the random vibration test. The LLSS test was performed with a 0.15 g sine load in the frequency range of 5 to 2000 Hz. Table 7 shows a comparison of the LLSS results for the S-STEP satellite before and after the random vibration test. By comparing the 1st peak frequency values before and after the random vibration test, it was determined that the frequency shift was below 5% (the pass/fail criterion of the vibration test). The LLSS results demonstrate that there was no structural deformation in the S-STEP satellite before or after the random vibration test. This indicates that the proposed concept of a multilayered high-damping CFRP-based patch can effectively ensure the structural stability of an S-STEP satellite under launch conditions and enable it to enter its mission orbit without the need for major modifications to the design of the satellite's primary structure. This vibration reduction mechanism also enables the completion of the production of the satellite according to the designated schedule.

Table 7. Results of the low-level sine sweep test conducted on the S-STEP satellite before and after the random vibration test.

Part	Status	1st Peak Frequency	Frequency Shift Difference (%)
CoG	Before Random After Random	36.3 35.4	2.47
Battery	Before Random After Random	27 26.3	2.59
PSU	Before Random After Random	26.5 25.4	4.15
SAR Ant.	Before Random After Random	27.2 26.2	3.68

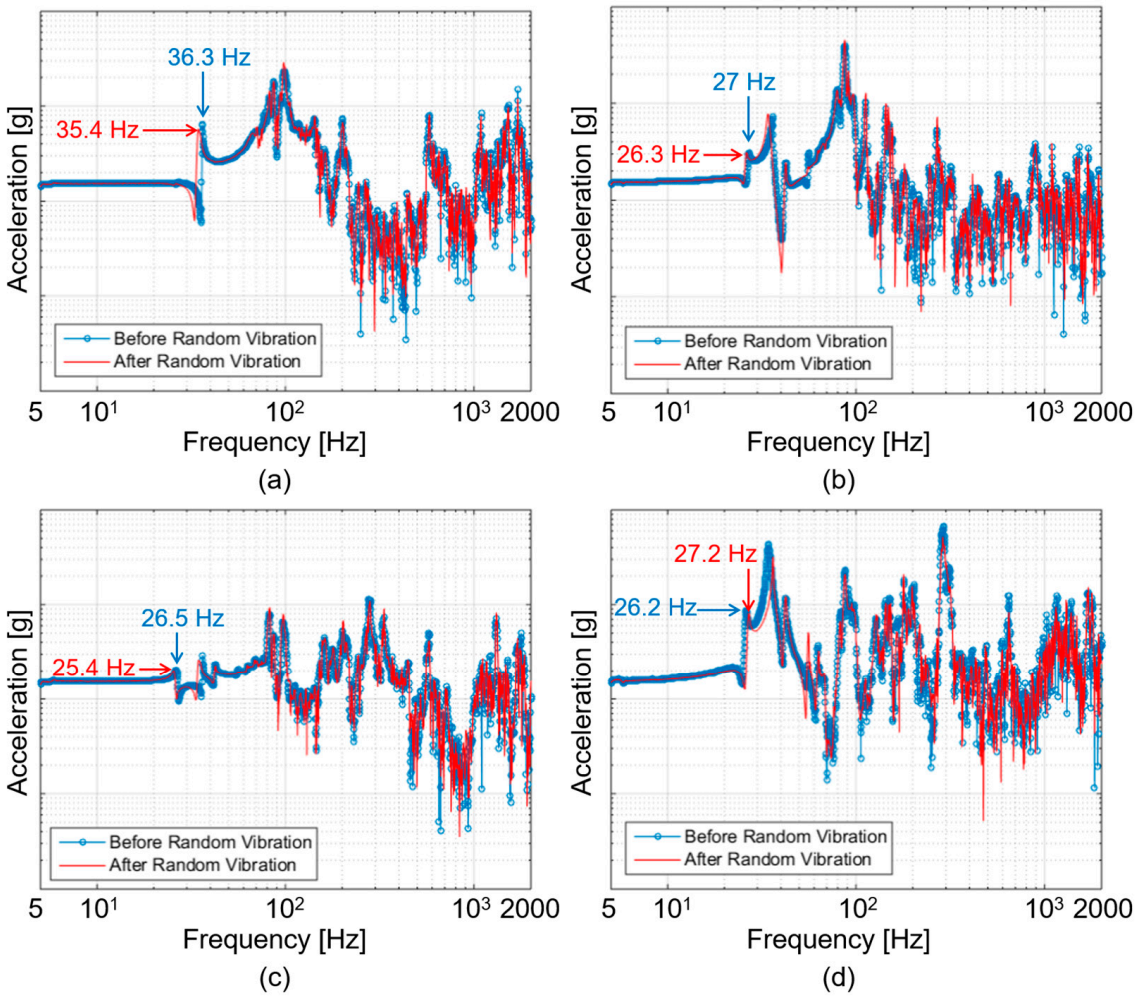

Figure 10. Results of the low-level sine sweep (LLSS) test conducted on the S-STEP satellite before and after the random vibration test measured at (**a**) the CoG, (**b**) the battery, (**c**) the power supply unit (PSU), and (**d**) the SAR antenna.

5. Conclusions

In this study, we developed an attachable vibration reduction structure to improve the structural dynamics of an active small SAR S-STEP satellite and reduce the structural vibrations generated by the dynamic loads generated in the launch environment without the need for any major design changes. In order to design the stacking sequence and determine the type of material we would use for the vibration reduction structure, the sine and random vibration reduction performances of the CFRP- and FR4-based patches were investigated at the specimen level. Next, lap shear tests were conducted to evaluate the adhesive stability of the damping tape. Finally, the structural stability of the S-STEP satellite with the CFRP-based patch was experimentally verified using sine and random vibration tests. The results obtained from the vibration and lap shear tests yielded the following conclusions:

(1) In the sine and random vibration tests, the acceleration and PDS response of S-STEP satellite satisfied the dynamic stability requirements of the vibrational test specification. The maximum acceleration response measured during the sine vibration test (15.02 g) was lower than the design load of the satellite (18 g). Additionally, the RMS value at the CoG (5.84 grms) measured during the random vibration test was lower than the input profile (6.09 grms).

(2) In the lap shear tests, the average shear strength of the specimens was approximately 8.28 MPa. Since the maximum shear stress obtained from the sine vibration analy-

sis was approximately 5.2 MPa, the multilayered high-damping CFRP-based patch was able to prevent delamination from occurring between the damping tape and CFRP plate.

The CFRP-based patch developed in this study enables the development of lightweight satellite structures with high stiffness and high vibration reduction performance relative to the added mass. It is possible to improve the structural stability of pre-manufactured satellite structures during a satellite's development process. The lightweight vibration reduction mechanism developed in this study is one of the best means of protecting vibration-sensitive components, such as the interface between the launch adaptor and the satellite, or the satellite structure, which is the fundamental framework for attaching components such as the battery, power supply unit, etc. Utilizing the attachable vibration reduction structure proposed in this study should enable active adaptation to the rapidly evolving new space industry ecosystem and ensure that the design, evaluation, and launch processes can be completed efficiently.

Author Contributions: Conceptualization, S.-C.K. and H.-U.O.; methodology, D.-G.K.; software, H.-G.K.; validation, D.-G.K., S.-C.K. and K.-R.K.; formal analysis, S.-C.K.; investigation, K.-R.K.; resources, H.-U.O.; data curation, H.-G.K.; writing—original draft preparation, H.-G.K.; writing—review and editing, D.-G.K. and S.-C.K.; visualization, H.-G.K.; supervision, K.-R.K. and H.-U.O.; project administration, K.-R.K. and H.-U.O.; funding acquisition, K.-R.K. and H.-U.O. All authors have read and agreed to the published version of the manuscript.

Funding: This research was supported by the Challengeable Future Defense Technology Research and Development Program (912777601-9127776-04) of the Agency for Defense Development (ADD) in 2022.

Data Availability Statement: Not applicable.

Conflicts of Interest: The authors declare no conflict of interest.

References

1. Bousedra, K. Downstream Space Activities in the New Space Era: Paradaigm Shift and Evaluation Challenges. *Space Policy* **2023**, *64*, 101553. [CrossRef]
2. Ince, F. Nano and micro satellites as the pillar of the "new space" paradigm. *J. Aeronaut. Space Technol.* **2020**, *13*, 235–250.
3. Kwon, S.-C.; Son, J.-H.; Song, S.-C.; Park, J.-H.; Koo, K.-R.; Oh, H.-U. Innovative Mechanical Design Strategy for Actualizing 80 kg-Class X-Band Active SAR Small Satellite of S-STEP. *Aerospace* **2021**, *8*, 149. [CrossRef]
4. Kim, H.-G.; Kwon, S.-C.; Koo, K.-R.; Song, S.-C.; Yu, Y.; Song, Y.; Park, Y.-H.; Oh, H.-U. New Performance Investigation of Superplastic Shape Memory Alloy-Based Vibration Isolator for X-Band Active Small SAR Satellite of S-STEP under Acoustic and Random Vibration Environments. *Aerospace* **2021**, *8*, 278.
5. Kim, S.; Song, C.-M.; Lee, S.-H.; Song, S.-C.; Oh, H.-U. Design and Performance of X-Band SAR Payload for 80 kg Class Flat-Panel-Type Microsatellite Based on Active Phased Array Antenna. *Aerospace* **2022**, *9*, 213. [CrossRef]
6. Wijker, J. *Random Vibrations in Spacecraft Structures Design: Theory and Applications*; Springer Science & Business Media: Berlin/Heidelberg, Germany, 2009; Volume 165.
7. Mani, M.; Naghib-Lahouti, A.; Nazarinia, M. Experimental and numerical aerodynamic analysis of a satellite launch vehicle with strap-on boosters. *Aeronaut. J.* **2004**, *108*, 379. [CrossRef]
8. Japan Aerospace Exploration Agency. Epsilon Launch Vehicle User's Manual. 2018. Available online: https://www.arianespace.com/vehicle/soyuz/ (accessed on 30 July 2023).
9. Arianespace. Vega-C User's Manual. 2018. Available online: https://www.arianespace.com/vehicle/vega-c/ (accessed on 30 July 2023).
10. Space X. Falcon 9 Users Guide. 2021. Available online: https://www.spacex.com/vehicle/falcon-heavy/ (accessed on 30 July 2023).
11. Arianespace. Ariane 6 User's Manual. 2021. Available online: https://www.arianespace.com/vehicle/soyuz/ariane-6/ (accessed on 30 July 2023).
12. Kwon, S.-C.; Jeon, S.-H.; Oh, H.-U. Performance evaluation of spaceborne cryocooler micro-vibration isolation system employing pseudoelastic SMA mesh washer. *Cryogenics* **2015**, *67*, 19–27. [CrossRef]
13. Kwon, S.-C.; Oh, H.-U. Passive micro-jitter isolation of gimbal-type antenna by using a superelastic SMA gear wheel. *Mech. Syst. Signal Process.* **2019**, *114*, 35–53.
14. Park, T.-Y.; Shin, S.-H.; Park, S.-W.; Kang, S.-J.; Oh, H.-U. High-damping PCB implemented by multi-layered viscoelastic acrylic tapes for use of wedge lock applications. *Eng. Fract. Mech.* **2021**, *241*, 107370.

15. Morgan, P. *Carbon Fiber and Their Composite Material*; CRC Press: Boca Raton, FL, USA, 2005.
16. Kumar, P.; Singh, S.P.; Sharma, S. *Damping in Fiber Reinforced Composite Materials*; Woodhead Publishing: Sawston, UK, 2023.
17. Qaderi, F.S.; Ebrahimi, M.V. Dynamic analysis of multi-layered composite beams reinforced with graphene platelets resting on two-parameter viscoelastic foundation. *Eur. Phys. J. Plus* **2019**, *134*, 339. [CrossRef]
18. Kim, M.-J.; Lee, J.-H.; Kim, S.-H.; Lee, C.-M.; Kim, D.-H. Comparative Analysis of CFRP and Steel Vibration Characteristics of Machine Tools Components. *Appl. Sci.* **2023**, *13*, 1083. [CrossRef]
19. Cho, H.K.; Rhee, J. Vibration in a satellite structure with a laminate composite hybrid sandwich panel. *Compos. Struct.* **2011**, *93*, 2566–2574. [CrossRef]
20. *ECSS-E-ST-10-03C*; ECSS Standard: Testing (31 May 2022). European Consortium for Space Standards: Noordwijk, The Netherlands, 2022. Available online: https://ecss.nl/standard/ecss-e-st-10-03c-rev-1-testing-31-may-2022/ (accessed on 30 July 2023).
21. *ASTM D 5868-01*; Standard Test Method for Lap Shear Adhesion for Fiber Reinforced Plastic (FRP) Bonding. Annual Book of American Society for Testing Materials. ASTM International: West Conshohocken, PA, USA, 2001; Volume 15, p. 518. Available online: https://www.astm.org/d5868-01r14.html (accessed on 30 July 2023).